REPORT DOCUMENTATION PAGE

Form Approved
OMB No. 0704-0188

1. REPORT DATE *(DD-MM-YYYY)*	2. REPORT TYPE	3. DATES COVERED *(From - To)*
22-09-2007	Technical Paper	

4. TITLE AND SUBTITLE

Operating Characteristics of Cylindrical and Annular Helicon Sources (Preprint)

5a. CONTRACT NUMBER

5b. GRANT NUMBER

5c. PROGRAM ELEMENT NUMBER

6. AUTHOR(S)
Brian E. Beal (AFRL/PRSS) and Fabian Mak (Georgia Tech)

5d. PROJECT NUMBER

5e. TASK NUMBER
33SP0708

5f. WORK UNIT NUMBER

7. PERFORMING ORGANIZATION NAME(S) AND ADDRESS(ES)

Air Force Research Laboratory (AFMC)
AFRL/PRSS
1 Ara Drive
Edwards AFB CA 93524-7013

8. PERFORMING ORGANIZATION REPORT NUMBER

AFRL-PR-ED-TP-2007-390

9. SPONSORING / MONITORING AGENCY NAME(S) AND ADDRESS(ES)

Air Force Research Laboratory (AFMC)
AFRL/PRS
5 Pollux Drive
Edwards AFB CA 93524-7048

10. SPONSOR/MONITOR'S ACRONYM(S)

11. SPONSOR/MONITOR'S NUMBER(S)
AFRL-PR-ED-TP-2007-390

12. DISTRIBUTION / AVAILABILITY STATEMENT

Approved for public release; distribution unlimited (PA #07325A).

13. SUPPLEMENTARY NOTES
For presentation at the 30th International Electric Propulsion Conference (2007 IEPC), Florence Italy, 17-20 Sep 2007. IEPC-2007-71.

14. ABSTRACT

The power required to create an ionized plasma is a significant energy loss mechanism in typical electric propulsion systems. The use of wave-driven helicon sources is one approach that has been considered as a means of reducing this loss due to the reportedly low ionization cost found in these devices. In order to extend the benefits of the helicon ionization mechanism to the widest possible array of devices, a program has been initiated to develop and demonstrate a helicon operating in an annular configuration. A 15-cm diameter helicon source has been operated on both argon and xenon gas at power levels ranging from 200W to 3.2 kW and magnetic field strengths up to 1.6 kG for both cylindrical and annular configurations. Measurements of the resultant plasma load impedance have revealed distinct transitions to a high-resistance, visually bright regime associated with operation in the helicon mode. The qualitative similarity of the load response for both geometric configurations supports the notion that helicon sources can be created in both cylindrical and annular modes.

15. SUBJECT TERMS

16. SECURITY CLASSIFICATION OF:			17. LIMITATION OF ABSTRACT	18. NUMBER OF PAGES	19a. NAME OF RESPONSIBLE PERSON
					Dr.James M. Haas
a. REPORT	b. ABSTRACT	c. THIS PAGE	SAR	18	19b. TELEPHONE NUMBER *(include area code)*
Unclassified	**Unclassified**	**Unclassified**			N/A

Operating Characteristics of Cylindrical and Annular Helicon Sources (Preprint)

Brian E. Beal
Air Force Research Laboratory, Edwards AFB, CA 93524

Fabian Mak
Georgia Institute of Technology, Atlanta, GA 30332

The power required to create an ionized plasma is a significant energy loss mechanism in typical electric propulsion systems. The use of wave-driven helicon sources is one approach that has been considered as a means of reducing this loss due to the reportedly low ionization cost found in these devices. In order to extend the benefits of the helicon ionization mechanism to the widest possible array of devices, a program has been initiated to develop and demonstrate a helicon operating in an annular configuration. A 15-cm diameter helicon source has been operated on both argon and xenon gas at power levels ranging from 200W to 3.2 kW and magnetic field strengths up to 1.6 kG for both cylindrical and annular configurations. Measurements of the resultant plasma load impedance have revealed distinct transitions to a high-resistance, visually bright regime associated with operation in the helicon mode. The qualitative similarity of the load response for both geometric configurations supports the notion that helicon sources can be created in both cylindrical and annular modes.

Nomenclature

B_0	=	magnitude of DC magnetic flux
c	=	speed of light in vacuum
e	=	electron charge
E_r	=	resonant energy
I_{sp}	=	specific impulse
k	=	axial wave number
L	=	length of half-wavelength antenna
m	=	azimuthal wave mode (integer)
m_e	=	electron mass
$\dot{m}_i$	=	propellant mass flow rate
M	=	ion mass
n_0	=	electron number density
$P_{ionization}$	=	ionization power
P_{input}	=	input electrical power
P_{thrust}	=	thrust power
r	=	radial coordinate
R_p	=	load resistance of antenna and plasma
v_φ	=	wave phase velocity
v_z	=	axial component of ion exit velocity (mass averaged)
T/P_{input}	=	thrust-to-power ratio
X_p	=	load reactance of antenna and plasma
z	=	axial coordinate
Z_{imag}	=	reactive part of Z_{tot}
Z_{real}	=	resistive part of Z_{tot}
Z_{tot}	=	combined impedance of the matching network, antenna, and plasma

IEPC-2007-71, International Electric Propulsion Conference, Florence, Italy, September 17-20, 2007

α = total wave number
η = thrust efficiency
η_{ideal} = ideal thrust efficiency
θ = azimuthal coordinate
μ_0 = permeability of free space
ω = angular frequency of wave
ω_c = electron cyclotron frequency
ω_{LH} = lower hybrid frequency
ω_p = electron plasma frequency
ξ = ionization cost (energy per ion)

I. Introduction

Electric propulsion (EP) systems are entering routine use for orbit topping and stationkeeping maneuvers onboard modern spacecraft. Due to their high specific impulse compared to chemical propulsion systems, EP devices offer significant reductions in the propellant mass required to perform a given mission. One of the most important figures of merit used to characterize the performance of an EP system is its thrust efficiency, which is a measure of how effectively input power from a spacecraft bus is transformed into propulsive thrust power. In its most fundamental form, the efficiency of a device can be written as shown in Eqn. 1.

$$\eta = \frac{P_{thrust}}{P_{input}} \tag{1}$$

With the exception of electrothermal thrusters, which function by heating a working gas and expanding it through a nozzle to create thrust in a manner that is similar to conventional rocket engines, most EP devices rely on the application of electric and magnetic fields to an electrically-charged propellant. While there are exceptions, most notably in the form of ionic liquids that are often used in micropropulsion devices, in many cases the "electrically-charged propellant" is first created by ionization of an initially neutral working fluid. The resultant plasma is then accelerated either electrostatically or electromagnetically. In such devices, the overall operation of the thruster can be divided into two main processes: ionization and acceleration. Although the physical mechanisms employed to induce ionization and acceleration vary as a function of the type of thruster considered, both processes inevitably require input power. Ignoring ancillary losses (e.g. heater power, thermal losses, beam divergence, etc.) that are specific to a given type of thruster, the maximum achievable efficiency can be written as in Eqn. 2, where the ionization and thrust powers are defined as shown in Eqns. 3 and 4.

$$\eta_{ideal} = \frac{P_{thrust}}{P_{thrust} + P_{ionization}} = \frac{1}{1 + \frac{P_{ionization}}{P_{thrust}}} \tag{2}$$

$$P_{ionization} \equiv \frac{\dot{m}_i \xi}{M} \tag{3}$$

$$P_{thrust} \equiv \frac{\dot{m}_i v_z^2}{2} \tag{4}$$

$$\frac{P_{ionization}}{P_{thrust}} = \frac{2\xi}{M v_z^2} = \frac{2\xi}{M\left(g I_{sp}\right)^2} \tag{5}$$

Equation 2 illustrates the intuitively obvious concept that the efficiency of a thruster is maximized when the ratio of ionization power to thrust power is minimized. This ratio, in turn, is shown by Eqn. 5 to be linearly related to the ionization cost, which is defined as the input energy required to produce a single ion. Although the theoretical minimum value of the ionization cost is a function of only the type of propellant gas used, the actual ionization cost is also dependent on the ionization mechanism employed and is often found to be several times greater than the theoretical minimum. For example, the DC bombardment mechanism employed by devices such as Hall thrusters and gridded ion engines typically results in an ionization cost that is approximately a factor of ten higher than the theoretical minimum.[1,2] Inefficiencies in the ionization process clearly result in a limitation on the ultimate efficiency that is achieved by EP devices at any operating condition. This limitation becomes more acute when one considers the effect of operating at reduced specific impulse. In many situations, a propulsive maneuver or orbit transfer must be conducted in a specified amount of time to achieve mission objectives. In such cases, there is a minimum thrust-to-power ratio that must be achieved to provide the spacecraft with a certain velocity increment in an allotted time period. As shown by Eqn. 6, operating at an elevated thrust-to-power ratio necessitates operating at reduced specific impulse. When combined with Eqns. 2 and 5, this relationship clearly indicates the reduction in maximum efficiency that results from operation at an elevated T/P ratio. Minimization of the ionization cost is therefore especially critical for achieving high efficiency operation in this regime.

$$T/P_{input} = \frac{2\eta}{gI_{sp}} \tag{6}$$

One approach that may be considered to improve the performance of EP devices is to replace or supplement the inefficient DC electron bombardment ionization mechanism with a more efficient ionization process. One device that appears promising is the helicon source, which functions by injecting RF energy in the presence of a static magnetic field to produce cylindrically-bounded whistler waves. These waves follow the dispersion relation shown in Eqn 7 and can exist in the frequency range given by Eqn. 8. Helicon sources are often regarded as one of the most efficient methods for producing a high-density, low-temperature plasma.[1,3,4] In fact, it has been claimed by some groups that the actual ionization cost in a helicon source can approach the theoretical minimum, which is the first ionization energy of the working fluid.[4] Others have reported actual ionization costs more than an order of magnitude higher for helicons operating on light gases.[5]

$$\frac{\alpha k}{\omega} = \frac{\mu_0 e n_0}{B_0} = \frac{\omega_p^2}{\omega_c c^2} \tag{7}$$

$$\omega_{LH} << \omega << \omega_c \tag{8}$$

In addition to some uncertainty in the true ionization cost in a helicon discharge, another factor that complicates integration of such a source with some EP devices is its cylindrical geometry. Until recently, all published works on helicon sources have focused on cylindrical configurations, which is understandable considering that satisfaction of the governing wave equations is accomplished by application of cylindrical boundary conditions in the presence of an axial magnetic field. The cylindrical geometry, unfortunately, is not readily suitable to straightforward integration with annular devices such as Hall thrusters and certain types of field-reversed configurations. Recent analysis, however, has revealed that helicon waves can also exist and be excited in an annular, rather than purely cylindrical, geometry.[2,6,7] In light of this, a program has been initiated to build and characterize an annular helicon source. The ultimate goals of this program are to:

- Experimentally validate the analytical result showing that helicons can exist in an annular configuration
- Measure the ionization cost, ξ, in a helicon source as a function of source geometry (cylindrical or annular), working gas type, antenna geometry, static magnetic field strength, and input power
- Develop a theoretical and experimental basis for designing cylindrical and annular helicon sources capable of achieving very low ionization costs; and

- Assess the viability of cylindrical or annular helicons to serve as ionization sources for a variety of plasma accelerators.

In this paper, initial efforts to establish helicons in both cylindrical and annular geometries are discussed. Basic operating characteristics of a helicon source operating at power levels ranging from 200 W to 3.2 kW at magnetic fields of 0 to 1.6 kG are revealed for operation on both argon and xenon gas. Plasma impedance characteristics inferred from the parameters of an RF matching network are compared to theoretical results predicting the basic behavior of helicon sources.[8]

II. Experimental Setup

A. Helicon Source

The main structural component of the helicon source used in this experiment is a quartz tube with an inner diameter of 15 cm, an outer diameter of 15.6 cm, and a length of approximately 1.2 m. When operated in annular mode, a Pyrex cylinder with an outer diameter of 10 cm is inserted along the centerline of the device to form an annular space with a channel width of 2.5 cm and a mean diameter of 12.5 cm. This inner cylinder can be removed and replaced as necessary to rapidly convert the source from cylindrical to annular mode and vice versa. In either geometric configuration, propellant gas is fed into the device using digital Unit mass flow controllers. With the present setup, mass flows up to 250 standard cubic centimeters per minute (sccm) of xenon or 750 sccm of argon can be achieved.

Figure 1. A 15-cm diameter helicon source.

The static magnetic field required for helicon operation is supplied by five large, water-cooled electromagnets having an inner diameter of approximately 25 cm. These magnets are connected in series and powered by a variable DC power supply with a maximum current rating of 500 A. The axial magnetic field profile resulting from this configuration is shown in Fig. 2. As shown, the variation in magnetic field magnitude was less than ±10% over most of the working volume. The average magnetic field strength was variable from 0 to over 1600 gauss.

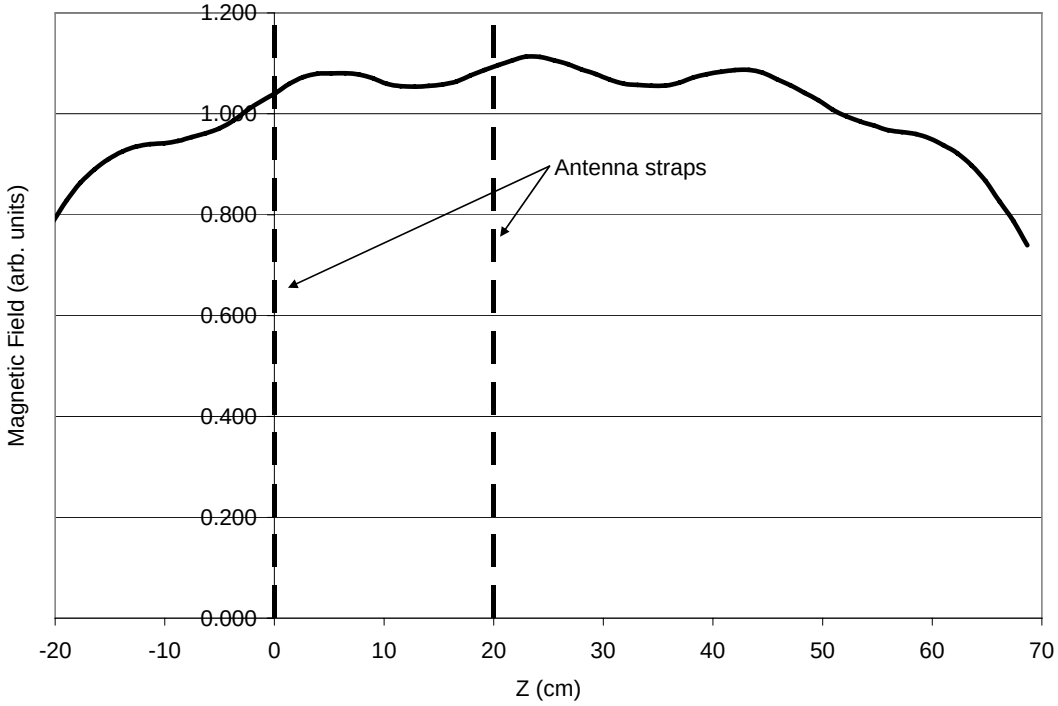

Figure 2. The axial magnetic field profile in the helicon source. Field values have been normalized to their average value for a given magnet current.

B. RF Power Circuit

The helicon used in this experiment was powered by an ENI model OEM-50 RF generator capable of outputting up to 5 kW at a fixed frequency of 13.56 MHz. The forward and reflected power delivered to the plasma were measured by a Bird 4421 power meter and 4027A10M sensor head. RF power was injected into the device via a double-strap m=0 antenna, where m is the azimuthal wave number describing the rotation of electric and magnetic wave fields according to Eqn. 9. This simple antenna consists of two circular copper straps surrounding the outer quartz tube and connected such that the RF currents in each strap are 180 degrees out of phase with each other. Although antennas designed to excite the m=1 mode have been reported to produce slightly higher plasma densities,[8,9] the symmetric m=0 mode antenna was chosen for this experiment due to its inherent simplicity and the ability to easily change the driving wavelength by simply changing the distance between the antenna straps. Except where otherwise noted, all measurements reported here were obtained with the antenna straps spaced 20 cm apart. The location of the antenna relative to magnetic field profile can be seen in Fig. 2. For cases where the antenna spacing was varied, the upstream strap (the one at z=0 in Fig. 2) was kept constant while the downstream strap was moved to obtain the desired antenna length.

$$\vec{B} = \vec{B}(r)\exp\left[i\left(m\theta + kz - \omega t\right)\right] \qquad \vec{E} = \vec{E}(r)\exp\left[i\left(m\theta + kz - \omega t\right)\right] \tag{9}$$

RF power was coupled to the antenna, and ultimately the plasma, via a Comdel CPM80 matching network. This network is a "T" type, capacitive network, and can be seen in Fig. 3, which also shows the overall RF circuit setup. In this matching network, the values of capacitors C_A and C_B are automatically tuned by a PID circuit in order to minimize reflected power and maximize the power delivered to the plasma. The shunt capacitor, C_{fix}, may be adjusted manually between runs, but was kept constant for the duration of this test.

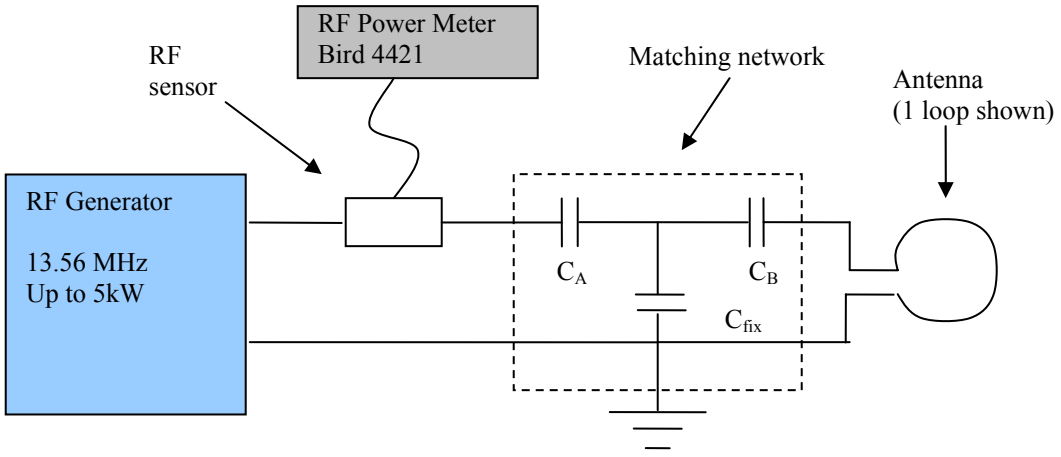

Figure 3. Electrical setup of helicon experiment.

In addition to matching the impedance of the antenna/plasma system to that of the RF generator, the matching network used in this experiment was also used as a rudimentary diagnostic. Because the RF generator is designed to deliver power to a 50Ω load, measurements of the capacitor values resulting in a well-matched system (i.e. a system in which the reflected power is low, typically less than 1% of the forward power) can be used to deduce the impedance of the loaded antenna and plasma. This is accomplished with the help of the equivalent circuit shown in Fig. 4, where R_P is the real (resistive) part of the load impedance and X_p is the imaginary (reactive) part. Using this model, the total, resistive, and reactive parts of the load impedance can be written as shown in Eqns. 10-12, respectively. By equating the real part of the impedance to 50Ω and the imaginary part to 0, the conditions that must be approached for a well-matched system, the resulting system of equations can be solved numerically to deduce the components of the load impedance in terms of C_A, C_B, and C_{fix}. It is worth noting that in this framework the impedance of the antenna itself is not explicitly separated from that of the plasma and hence the "load impedance" is that of the antenna and plasma combined.

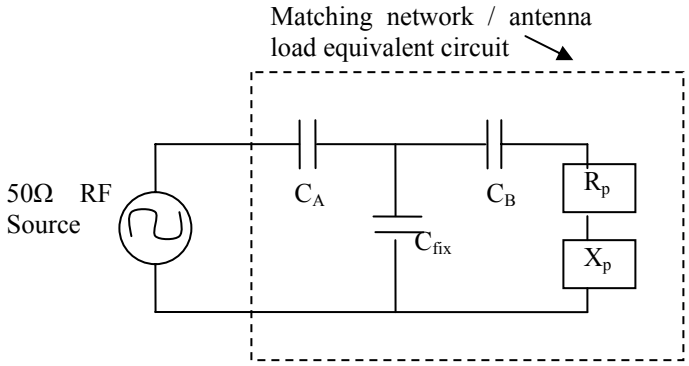

Figure 4. Equivalent circuit for assessing the load impedance of the antenna and plasma.

$$Z_{tot} = Z_{real} + iZ_{imag} \tag{10}$$

$$Z_{real} = \frac{R_p\left(\frac{X_p}{\omega C_{fix}} - \frac{1}{\omega^2 C_B C_{fix}} - \frac{\chi}{\omega C_{fix}}\right)}{R_p^2 + \chi^2} \tag{11}$$

$$Z_{imag} = \frac{\chi\left(\frac{1}{\omega^2 C_B C_{fix}} - \frac{X_p}{\omega C_{fix}}\right) - \frac{R_p^2}{\omega C_{fix}}}{R_p^2 + \chi^2} - \frac{1}{\omega C_A} \tag{12}$$

where $$\chi \equiv X_p - \frac{1}{\omega C_B} - \frac{1}{\omega C_{fix}} \tag{13}$$

C. Vacuum Chamber

For these experiments, the helicon source was attached to Chamber 5A at the Air Force Research Laboratory (AFRL) via a mechanical bellows as shown in Fig. 1. Chamber 5A is a diffusion-pumped, stainless steel vacuum chamber measuring approximately 1.5m in diameter and 1.8m in length. This chamber typically achieves a base pressure of approximately 2.5×10^{-4} Torr as indicated by a cold cathode gauge calibrated for air. When 100 sccm of argon is flowed into the system, the background pressure rises to approximately 5×10^{-3} Torr.

III. Results

As an initial test of the experimental setup, the helicon was first operated in a cylindrical mode on both xenon and argon gases. Measurements of load impedance were obtained and compared to both theoretical predictions and experimental values obtained by other groups to verify that a helicon plasma (as opposed to a capacitively- or inductively-coupled discharge) could be obtained. This was first accomplished by flowing 100 sccm of argon into the cylindrical helicon and observing the response of the plasma load to changes in magnetic field strength, applied RF power, and antenna spacing. Figure 5, below, shows the measured load resistance and reactance as a function of applied magnetic field strength. As the magnetic field strength is increased at constant applied power, the load resistance initially rises to a peak at approximately 50-100G before decreasing and asymptoting to near its zero field value as the magnetic field is increased further. Similarly, the load reactance initially rises to a maximum around 50-100G before declining and leveling off at a value approximately halfway between the zero field condition and the maximum.

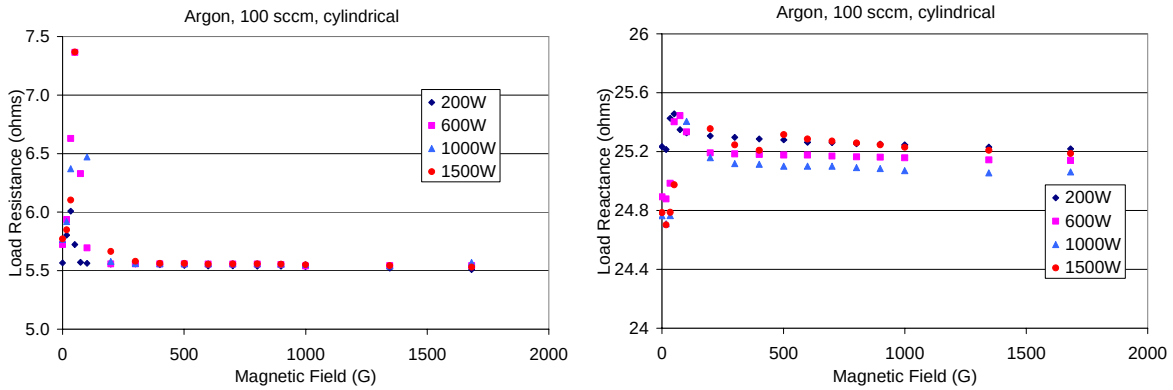

Figure 5. Load impedances for a 15-cm diameter, cylindrical helicon discharge operating with an argon flow of 100 sccm..

The behavior shown above can be compared to the analytical results of Shamrai, *et al.* who have calculated the load impedance of an m=0 mode antenna coupled to a helicon plasma with similar, though not identical, geometry. These predictions are shown in Fig. 6. Comparison of the experimental results to the analytical predictions is difficult due to the fact that the plasma density is not yet known for the experimental case. In the absence of

experimental plasma density values, there are two limiting cases that may be considered: constant density or density scaling linearly with magnetic field strength. The case of constant density corresponds to a situation in which the static magnetic field has no significant effect, that is in the case of a non-resonant capacitive discharge. In this case, one would expect the load resistance to show multiple peaks as the magnetic field is increased. Clearly this is not the trend displayed in Fig. 5. The other limiting case where density is proportional to applied magnetic field strength is expected to more closely resemble the actual situation. This can be deduced by first noting that the dispersion relation given as Eqn. 7 predicts a linear relation between these parameters for constant values of wavenumber and frequency. Second, the predicted linear relationship between density and magnetic field has been observed previously for RF discharges operating in the helicon mode. In this case, one may expect the load resistance to initially increase with magnetic field as the discharge transitions from a non-resonant inductive mode to the wave-driven helicon mode. Following transition to helicon mode, the resistance could then remain nearly constant as density increases linearly with magnetic field along the low-resistance, constant n/B trajectories shown in Fig. 6. Thus, the behavior displayed in Fig. 5 is consistent with, though certainly not conclusive proof of, operation in helicon mode.

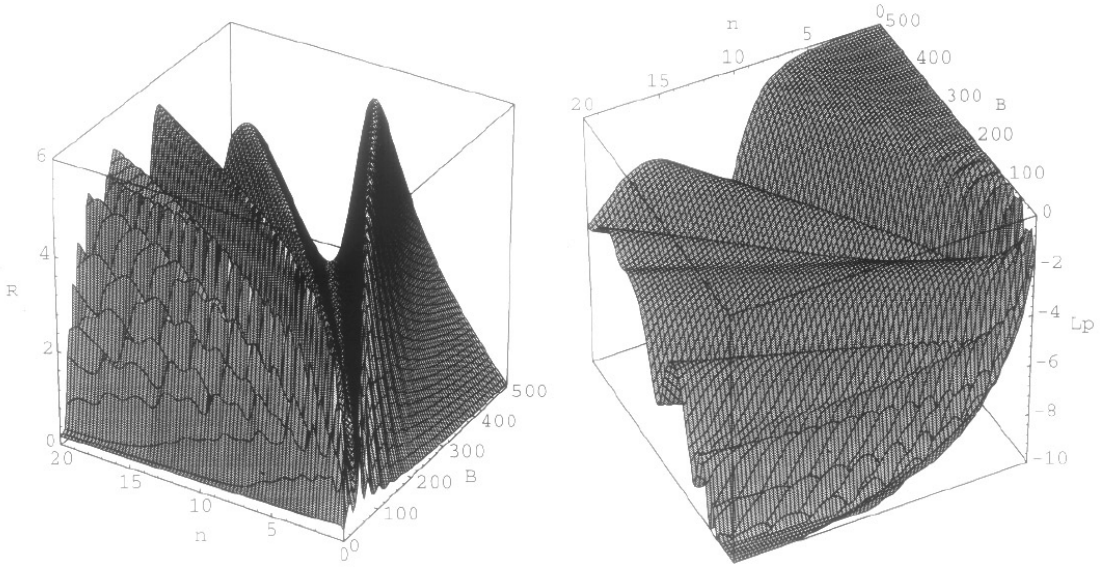

Figure 6. Analytical predictions of load impedance behavior for a 12.5-cm-diameter, helicon source excited with an m=0 antenna and operated with an argon pressure of 1 mTorr (from Ref. 8). Resistance (R) and inductance (L_p) are shown as a function of plasma density (n, in 10^{11} cm^{-3}) and magnetic field (B, in Gauss).

Following the experiments varying magnetic field strength, a brief set of experiments was conducted in which magnetic field strength and argon flow rate were held constant while RF power was varied. The resulting load impedances are given in Fig. 7 and show a nearly constant resistance until a distinct jump occurring at high power. The power level at which the increase in resistance is manifested is approximately 2.8 kW for a 500G field and roughly 3.2 kW for a 1000G field. Pictures of the discharge at various power levels are shown in Fig. 8. As one would expect, the visual brightness of the plasma increases with increasing power. At the highest power setting of 3.0 kW, the axial extent of the bright plasma column extends noticeably. The distinct visual transition to this mode occurs at the same time as the pronounced increase in load resistance shown in Fig. 7. This transition behavior is qualitatively similar to the jumps in plasma density that have been commonly reported as power is increased in an RF discharge.[10,11] Ellingboe and Boswell have attributed this behavior to transition from a non-resonant, inductively coupled plasma mode to a helicon mode.[12] The reproduction of this behavior in the present experiment suggests that a true helicon discharge is indeed being achieved, at least for the highest power experimental conditions.

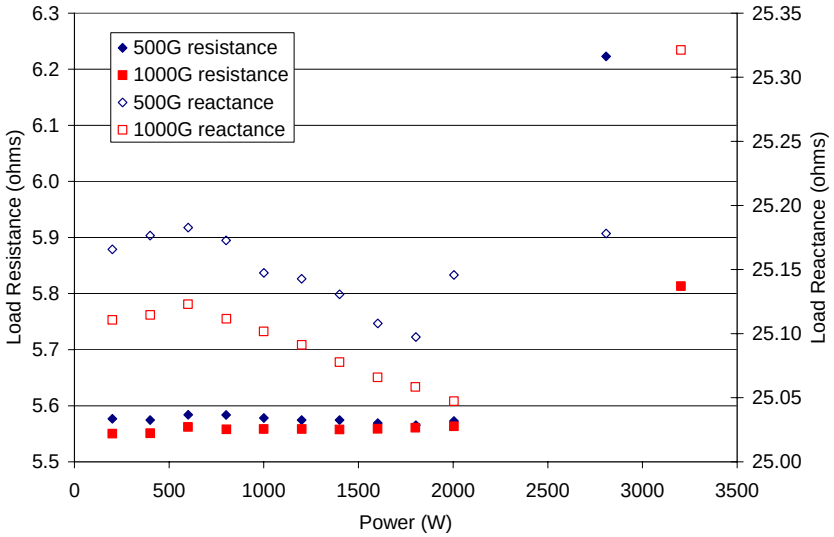

Figure 7. Impedance of a 15-cm diameter RF discharge as a function of applied power for constant magnetic field strength and an argon flow rate of 100 sccm.

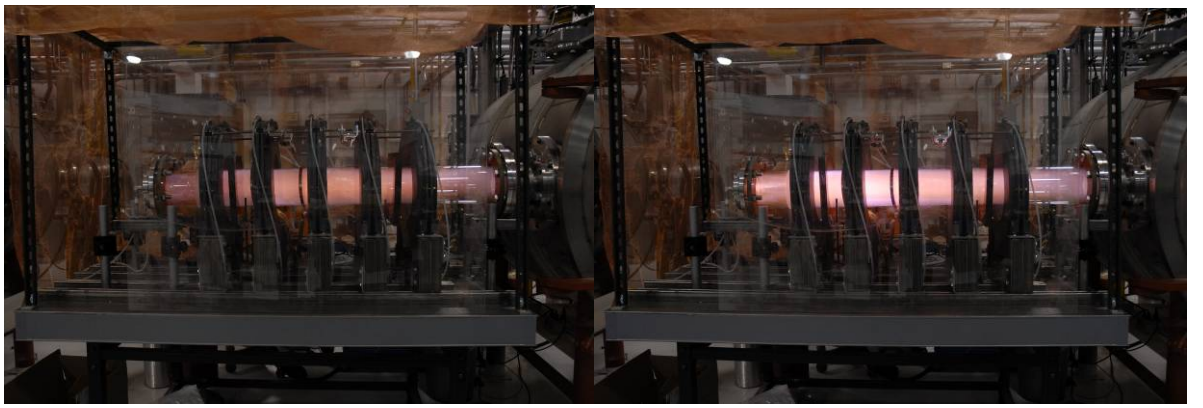

a. **b.**

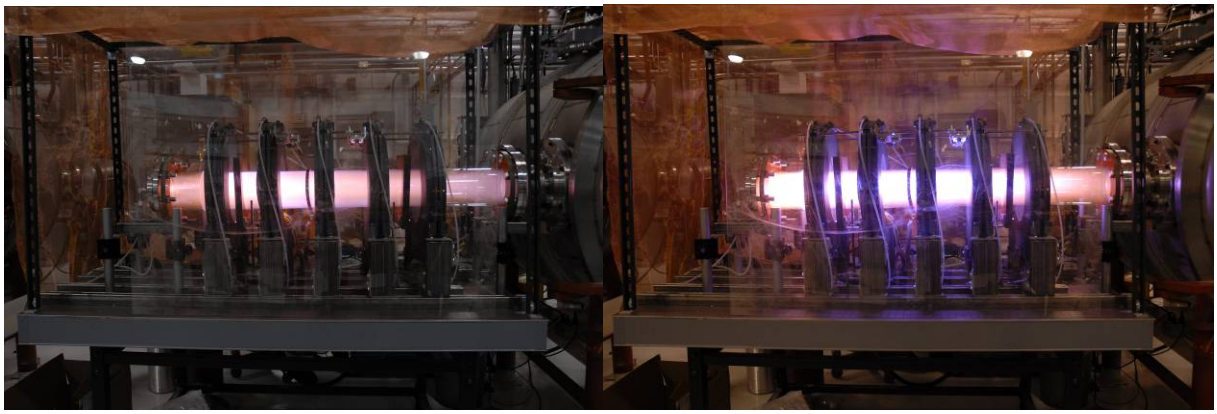

c. **d.**

Figure 8. An RF discharge at various power levels for a constant magnetic field of 500G and an argon flow rate of 100 sccm. The applied power levels were a.) 200W, b.) 1000W, c.) 2000W, and d.) 3000W.

The final parametric variation that was conducted was a limited study of the effect of antenna length on helicon operation. This was done in order to study the effect of varying the phase velocity, defined by Eqn. 14, of the driving wave.* Variation of the phase velocity, in turn, modifies the resonant energy, which is defined as in Eqn. 15 and represents the energy at which electrons are resonant with a wave of angular frequency ω and wavenumber k. For electrons that satisfy this condition, energy may be transferred directly to the electrons via wave-particle interaction. The effect of the antenna geometry on resonant wave energy may thus be expected to affect the ionization efficiency in a helicon device and to result in a peak in ionization rate when the resonant energy dictated by the antenna geometry matches the peak in the ionization cross-section of the working gas. There are several factors, however, that cause the operation of helicon sources to be less sensitive to antenna geometry than would otherwise be expected. First, although an m=0 mode antenna is designed to excite one primary wavelength, it can and does excite a fairly wide spectrum of k values.[13] Second, although the dispersion relation shown in Eqn. 7 is valid for helicon sources, the values of wavenumber, k, and density, n, are not necessarily spatially uniform throughout the plasma column. The ability of the plasma to vary spatially provides an additional degree of freedom by which the plasma may adjust to variations in antenna geometry while still maintaining a helicon discharge. Finally, in contrast to early theories of helicons, recent studies indicate that the main ionization mechanism in a helicon discharge is via mode coupling whereby a lightly-damped helicon wave transfers energy to a heavily-damped, electrostatic Trivelpiece-Gould (TG) wave, which in turn transfers energy to plasma electrons.[14,15] The fact that wave energy is coupled to the plasma via an indirect channel rather than as a result of direct Landau damping of the helicon wave itself suggests that the ionization efficiency of the source should be less dependent on the wave phase velocity than if the reverse were true. Nontheless, previous experiments have found that large changes in antenna geometry do indeed result in modest changes in plasma density. For that reason, the effect of antenna geometry was briefly considered in the present study.

$$v_\phi \equiv \frac{\omega}{k} \approx \frac{\omega L}{\pi} \tag{14}$$

$$E_r \equiv \frac{1}{2} m_e v_\phi^2 \tag{15}$$

The separation between antenna straps was varied from 10 to 40 cm and at each value the applied RF power was varied at a constant applied magnetic field strength of 1000G. The resulting impedance response is shown in Fig. 9. As shown, at low values of applied RF power the resistance of the load is nearly constant for all values of L. As power is increased, however, the longest antenna spacing (40 cm) resulted in transition to the bright, high-resistance mode of operation at a lower power level (~2.8 kW) than the nominal (20 cm) antenna spacing, which required 3.2 kW of input power.

* The approximate equality in Eqn. 14 is valid only for the primary wavenumber excited by a half-wavelength antenna. The phase velocity in the plasma is not constrained to equal the phase velocity excited by the antenna, which is the one given by Eqn. 14.

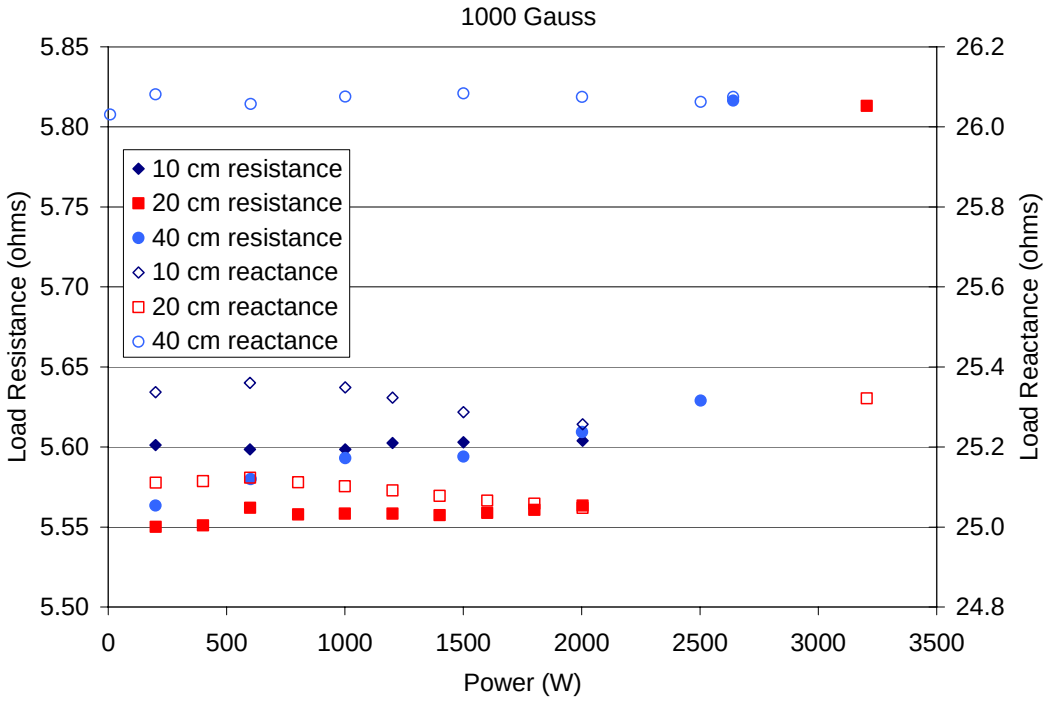

Figure 9. Impedance response of a 15-cm diameter, cylindrical helicon source operating on argon as power is varied for three different m=0 mode antenna geometries. The spacing between the antenna straps corresponds to half the length of the main wavelength excited by the symmetric antenna.

After concluding the initial checkout of the cylindrical source using argon propellant, the experiments were repeated using xenon. While argon gas has been the most prevalent working fluid for helicon experiments reported in the literature, xenon is a more common propellant for electric propulsion applications due to its higher atomic mass which normally translates to higher thrust levels for a given power level. The response of plasma impedance to changes in magnetic field strength is shown in Fig. 10 for a cylindrical source operating on a xenon flow of 100 sccm. The trend of load resistance versus magnetic field is qualitatively similar to the one shown in Fig. 5 for operation on argon. A notable difference, however, is that the high resistance peak is significantly wider for operation on xenon, particularly at high RF power levels.

Figure 11 shows the resistance and reactance of the xenon plasma load as the RF power is varied at constant magnetic field and propellant flow rate. The trend in resistance, including the discontinuous jumps that occur as power is increased, is similar to the behavior shown in Fig. 7 for operation on argon with one notable exception. Operation on xenon results in a resistance increase, and an accompanying increase in the visible brightness of the plasma, at a significantly lower applied power than operation on argon. Figure 12 shows the impedance of the load as a function of power for three different antenna lengths and a constant magnetic field strength of 1000G. Here it can be seen that the xenon helicon source transitioned to a high-resistance, visually bright plasma mode at an input RF power of 600-1000W for each of the three antenna configurations. Comparison of Fig. 12 with Fig. 8 shows that the transition occurs at lower power levels for xenon operation than for argon operation regardless of the antenna geometry. It can therefore be concluded that the difference in transition power is not an effect of fortuitous antenna length selection. In other words, it is not the case that the selected antenna length is "more optimal" for xenon than argon since the transition power was only weakly influenced by variations in antenna geometry.

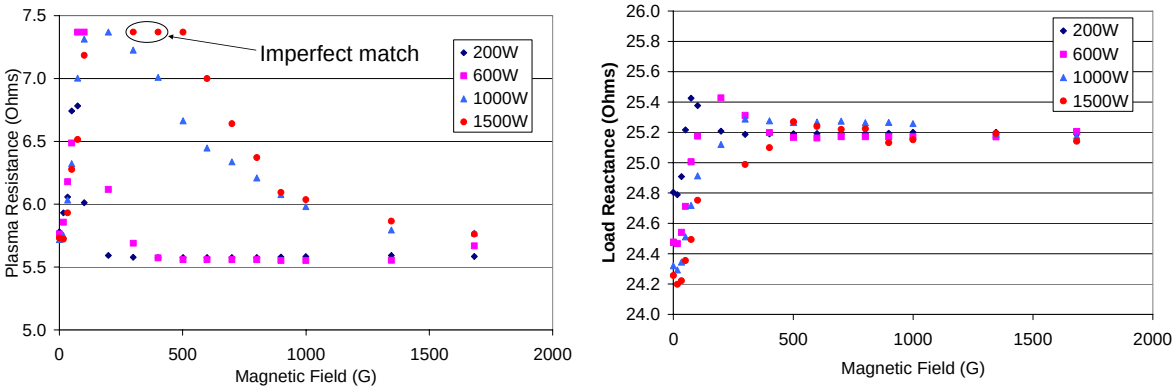

Figure 10. Load impedances for a 15-cm diameter, cylindrical helicon discharge operating with a xenon flow of 100 sccm. Note the differences compared to Fig. 5, which are a result of changing the working gas from argon to xenon.

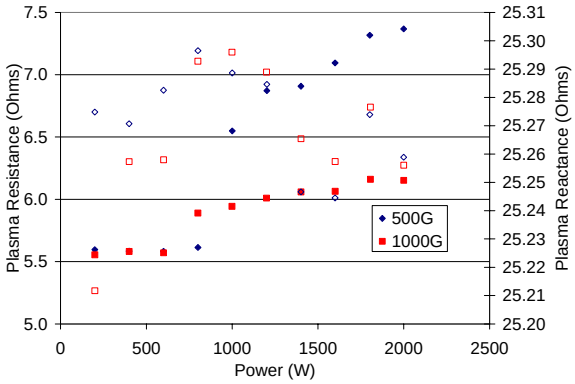

Figure 11. Impedance of a 15-cm diameter RF source as a function of applied power for constant magnetic field and a xenon flow rate of 100 sccm.

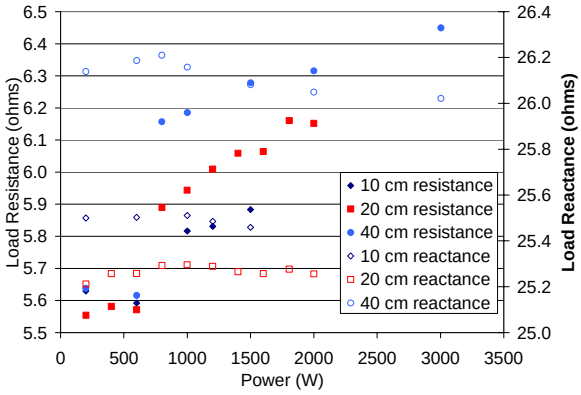

Figure 12. Impedance of a 15-cm diameter, cylindrical helicon operating on xenon with three different m=0 antenna lengths.

The observed trend showing mode transition at lower powers for operation on xenon and higher powers for operation on argon is not fully understood, but it may be an artifact of a sensitivity to particle pressure in the source. Experiments conducted by other groups have revealed that cylindrical sources operated on argon achieve transition to a high-density, high-resistance mode at lower threshold powers when operated at elevated pressures.[16] This phenomenon has been theorized to be a result of increased wave damping rates stemming from elevated electron collision rates that occur at high pressure, although experimental data confirming this hypothesis are limited.[17]

As an initial test of this hypothesis, the load resistance of the source was recorded as a function of propellant flow rate for both argon and xenon at a constant RF power of 1.5 kW and a magnetic field strength of 1000G. Experimentally, there are two quantities that can be matched when comparing the flow rates of different gases: the volumetric (particle) flow rate and the mass flow rate, which of course differ as a function of the atomic mass of the working gas. Both perspectives are shown in Fig. 13, which reveals that both argon and xenon result in resistance jumps as gas flow rate is increased. For xenon operation the transition occurs at a low flow rate of 37.5 sccm (~3.7 mg/s) and is followed by a linear increase in load resistance with increasing flow. Argon operation, on the other hand, results in a relatively high transition flow rate of 350 sccm (~5.8 mg/s), which is followed by a nearly constant resistance as flow is increased. The fact that the previously studied flow rate of 100 sccm was above the critical flow rate for xenon, but below it for argon suggests that the high power needed for argon transition (see Fig. 7) could be reduced by operating at higher flow rates. That this is indeed the case is shown by Fig. 14, which gives the load impedance as a function of power for operation at an elevated argon flow rate of 328.5 sccm, which is the same mass flow rate (~9.8 mg/s) as that shown previously for xenon operation at a volumetric flow rate of 100 sccm. At

this elevated argon flow rate, transition to the high resistance, high brightness mode occurs at an RF power of 1.6 kW as opposed to the 3.2 kW that was required at 100 sccm. Although the effect of flow rate is not yet well understood, empirical evidence clearly shows this parameter to have a pronounced effect and therefore it will be a subject of future study.

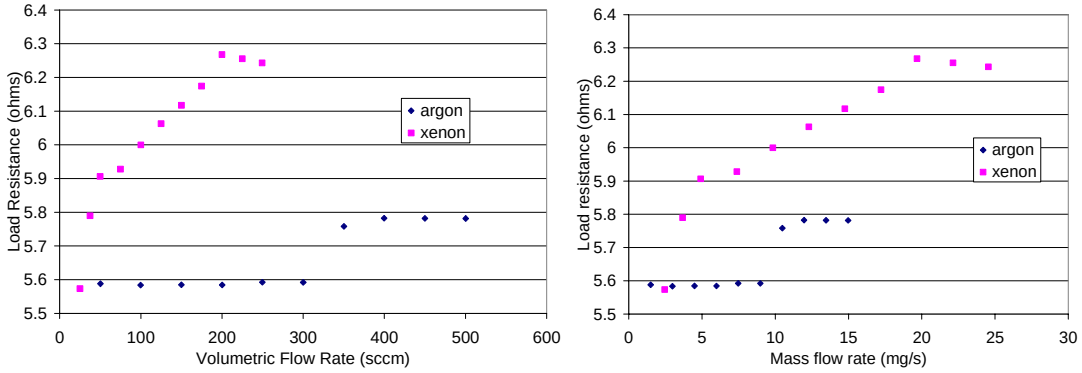

Figure 13. The load resistance of cylindrical helicon sources as a function of gas flow rate for an incident power of 1.5 kW and magnetic field of 1000G.

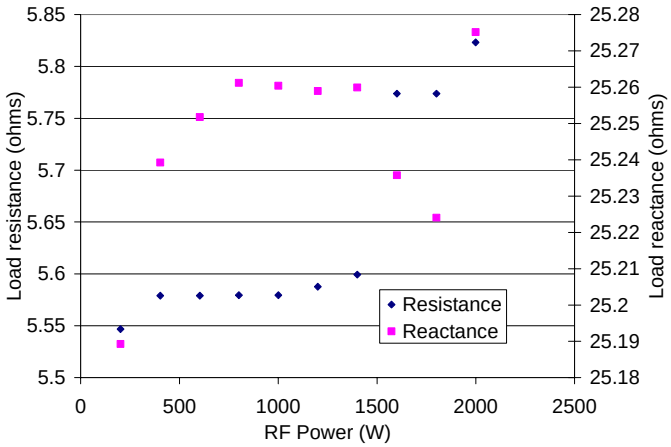

Figure 14. Impedance of a cylindrical helicon source as a function of applied power for a magnetic field of 1000G and an argon flow rate of 328.5 sccm.

After thoroughly examining the operating space for a cylindrical helicon, the source was transitioned to an annular mode and the experiment repeated. The main goal of this configuration was to verify that the qualitative behavior of the annular source is qualitatively similar to that of cylindrical sources and thereby offer initial support for previously published analytical studies showing that helicons can exist in an annular geometry.[2,6,7] As a first check of this, the load resistance was measured as a function of magnetic field strength for constant power and gas flow rate (100 sccm). The results, shown in Fig. 15, can be directly compared to the results from the cylindrical mode, which were given in Figs. 5 and 10. Comparison of these figures shows that the behavior of the annular source is very similar to that of the cylindrical one. Specifically, operation on either gas results in a peak in load resistance at a low magnetic field of approximately 50-100G. This peak is followed by a decline to near the zero-field resistance values. Just as in the cylindrical configuration, operation on xenon results in an elevated resistance regime that extends over a wider range of magnetic fields than that resulting from operation on argon. In Fig. 15, the few data points where the impedance match was poor (i.e. when the reflected power exceeded 5% of the incident power), are annotated. In the case of imperfect impedance matching, the assumptions leading to the derivation of Eqns. 11 and 12 are invalid and hence the inferred load resistances are unreliable.

The second parameter that was varied in the annular configuration was power. Figure 16 shows the effect of varying power for both xenon and argon (2 flow rates) at two different magnetic field settings. The left plot, which shows the response during operation on argon, is qualitatively similar to that exhibited by the cylindrical configuration. For the low flow (100 sccm) case, the trend is similar to that shown in Fig. 7 in that the load resistance is nearly constant with increasing power up to the maximum power examined, which was 2 kW. For the high flow (328.5 sccm) case, the results can be compared with Fig. 14. In both cases, the resistance initially showed

a linear increase with power followed by a nearly flat region as power was increased to about 1.5 kW. At this point, the cylindrical discharge exhibited an abrupt transition to a high-resistance, high-brightness mode of operation while the annular configuration showed a linear trend where both resistance and visual brightness increased smoothly with increasing power. The response of the xenon load impedance shown on the right side of Fig. 16 can be compared directly to Fig. 11, which shows data taken in the cylindrical configuration. In both cases, an initial trend where resistance increases slowly with applied power is followed by a steep increase. For the cylindrical case, the transition occurs at approximately 800-1000W of applied power while for the annular case the required power is roughly 200W higher. The visual changes that occur as power is increased can be seen in Fig. 17.

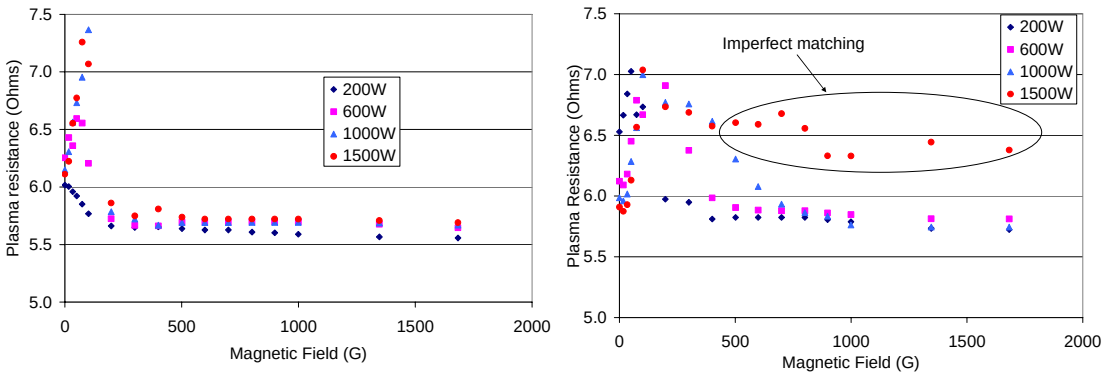

Figure 15. The load resistance of an annular helicon source as a function of magnetic field strength for 100 sccm flows of argon (left) and xenon (right).

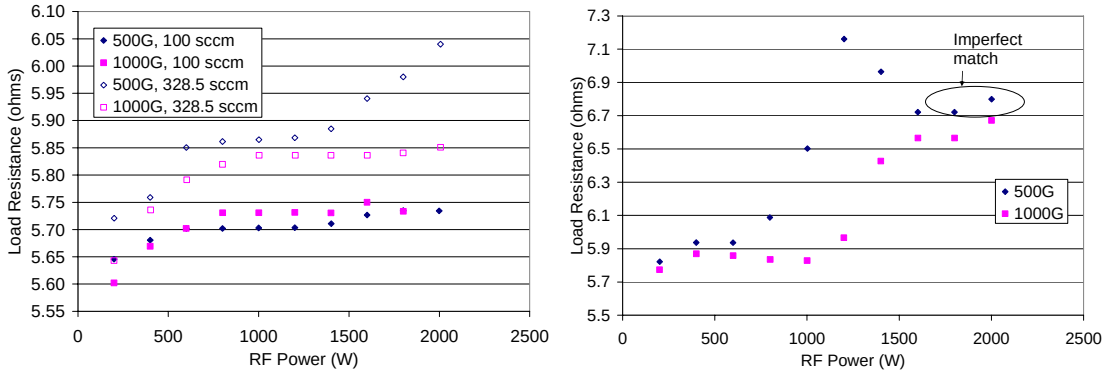

Figure 16. The load resistance of an annular helicon source as a function of RF power for operation on argon (left) and xenon (right).

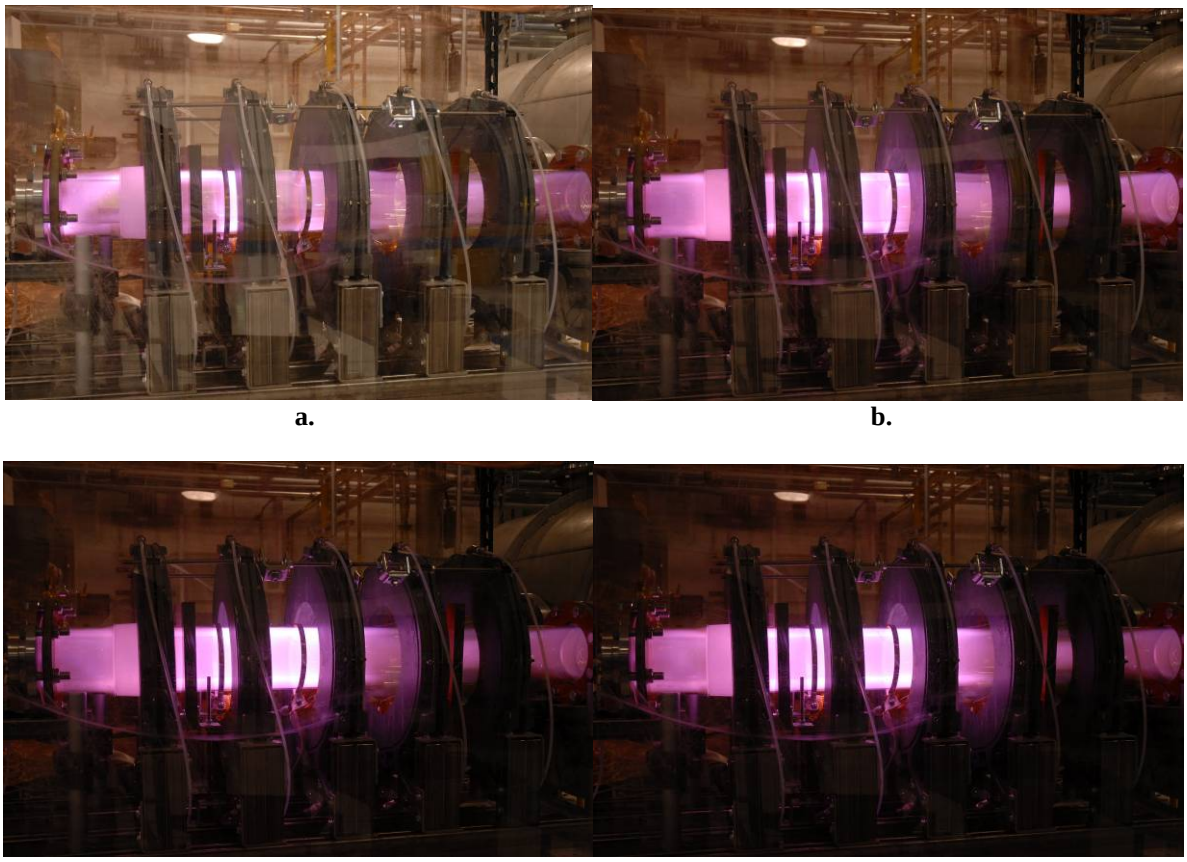

a. **b.**

c. **d.**

Figure 17. An annular helicon at various power levels for a constant magnetic field of 1000G and a xenon flow rate of 100 sccm. The applied power levels were a.) 200W, b.) 1000W, c.) 1500W, and d.) 2000W.

Finally, for the sake of completeness, the distance between the antenna straps was varied and the load impedance was recorded as a function of power for the annular configuration. The results are shown in Fig. 18, where the applied magnetic field was 1000G in each case. As for the cylindrical case, operation on argon reveals a nearly flat resistance versus power curve for input power levels up to 2 kW. Xenon operation on the other hand

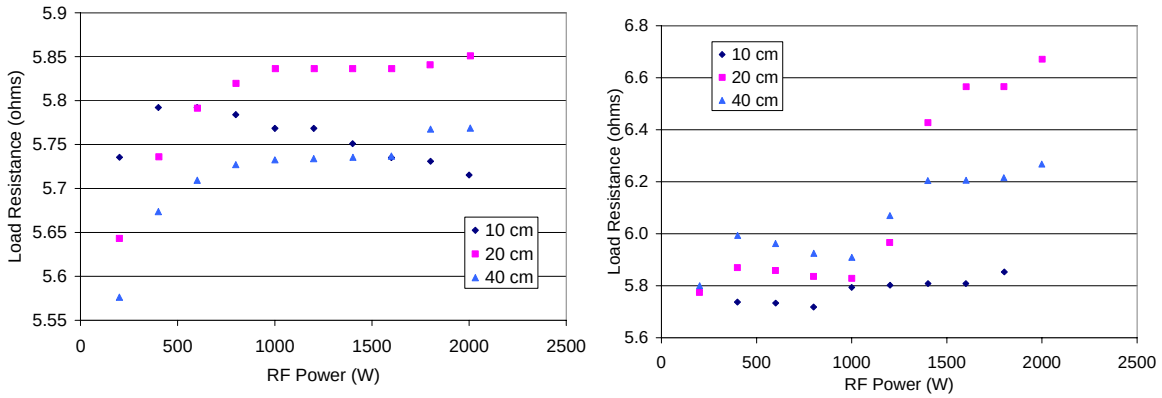

Figure 18. The response of an annular helicon source to changes in RF power and antenna length. The left plot shows operation with 100 sccm of Ar flow while the right is for the same flow rate of Xe.

results in a steep increase resistance once a critical power level is reached. As in the cylindrical case, the transition power is similar (within ~200W) between the three antenna lengths.

IV. Future Work

Having demonstrated that helicon plasma sources can be operated over a wide range of gas flows, magnetic field strengths, and power levels for both cylindrical and annular geometries, future work will soon turn toward application of standard plasma diagnostics to assess the ionization cost in the source as a function of key input parameters. The first step in this process will be to make detailed measurements of plasma density and electron temperature so that these values may be combined with an analytical diffusion model to estimate ionization costs. These measurements will be accomplished by a combination of emission spectroscopy and an RF-compensated Langmuir probe. Pending results of those measurements, a microwave interferometer may also be employed. Finally, direct measurements of ion escape flux will be attempted by using a negatively biased probe to measure the thermal flux of ions near the exit of the device. Following assessment of these data, additional plasma diagnostics will be employed as warranted.

In addition to the planned plasma measurements, future work will also include analysis of the power deposition mechanism and, in particular, consideration of how the annular geometry may influence the power deposition profile. Analysis of the antenna coupling mechanism may reveal the utility of examining azimuthal modes other than the m=0 one that was chosen for initial efforts primarily due to its experimental simplicity and flexibility.

V. Conclusion

Operation of cylindrical and annular RF plasma sources has revealed qualitatively similar behavior for both cases. The measurements of load resistance as a function of input power, magnetic field strength, and gas flow rate have revealed distinct transitions to a high-resistance, visually bright plasma mode associated with transition to a wave-resonant helicon discharge. Such measurements have shown the plasma response to be strongly dependent on magnetic field, gas type and flow rate, and input power, but only weakly dependent on the length of the driving antenna. The similarity of the response exhibited by the annular source to that of the cylindrical one supports, but does not yet conclusively prove, the previously reported analysis suggesting that true helicons can be created in an annular configuration as well as the traditional cylindrical geometry.

Acknowledgments

The authors would like to thank Professor Alec Gallimore of the University of Michigan for loaning us the large electromagnets used in this test. The use of these magnets saved us significant amounts of both time and effort in establishing the experimental setup. We also thank Professor Mitchell Walker of the Georgia Institute of Technology for useful discussions over the course of this project.

References

[1] F.F. Chen, "Experiments on helicon plasma sources," Journal of Vacuum Science and Technology A, Vol. 10, No. 4, July-Aug., 1992.

[2] B. Beal, A. Gallimore, D. Morris, C. Davis, and K. Lemmer, "Development of an Annular Helicon Source for Electric Propulsion Applications," AIAA-2006-4841, 42nd AIAA/ASME/SAE/ASEE Joint Propulsion Conference & Exhibit, Sacramento, CA, July 9-12, 2006.

[3] F.F. Chen, "Helicon Plasma Sources," in High Density Plasma Sources, edited by Oleg A. Popov, Noyes Publications, Park Ridge, NJ, Chap. 1, 1995.

[4] F.F. Chen, "Plasma Ionization by Helicon Waves," Plasma Physics and Controlled Fusion, Vol. 33, No. 4, pp. 339-364, 1991.

[5] E.A. Bering III, M. Brukardt, J.P. Squire, T.W. Glover, V. Jacobson, and G. McCaskill, "Recent Improvements in Ionization Costs and Ion Cyclotron Heating Efficiency in the VASIMR Engine," AIAA-2006-766, 44th AIAA Aerospace Sciences Meeting and Exhibit, Reno, NV, January 9-12, 2006.

[6] M. Yano and M.L.R. Walker, "Plasma ionization by annularly bounded helicon waves," Physics of Plasmas, Vol. 13, 063501, 2006.
[7] M. Yano and M.L.R. Walker, "Generalized theory of annularly bounded helicon waves," Physics of Plasmas, Vol. 14, 033510, 2007.
[8] K.P. Shamrai, V.P. Pavlenko, and V.B. Taranov, "Excitation, conversion and damping of waves in a helicon plasma source driven by an m=0 antenna," Plasma Physics and Controlled Fusion, Vol. 39, 1997, pp. 505-529.
[9] F.F. Chen, X. Jiang, and J.D. Evans, "Plasma injection with helicon sources," J. Vac. Sci. Technol. A, Vol. 18, No. 5, Sep-Oct 2000, pp. 2108-2115.
[10] F.F. Chen and R.W. Boswell, "Helicons – The Past Decade," IEEE Transactions on Plasma Science, Vol. 25, No. 6, Dec. 1997, pp. 1245-1257.
[11] A.J. Perry, D. Vender, and R.W. Boswell, "Application of the helicon source to plasma processing," J. Vac. Sci. Technol. B, Vol. 9, 1991, p. 310.
[12] A.R. Ellingboe and R.W. Boswell, "Capacitive, inductive and helicon-wave modes of operation of a helicon plasma source," Physics of Plasmas, Vol. 3, 1996, p. 2797.
[13] K.P. Shamrai and S. Shinohara, "Spectral and spatial characterization of a radio frequency power absorption in high pressure helicon plasmas," Physics of Plasmas, Vol. 8, No. 10, Oct. 2001, pp. 4659-4673.
[14] F.F. Chen and D. Arnush, "Generalized theory of helicon waves. I. Normal modes," Physics of Plasmas, Vol. 4, No. 9, Sept. 1997, pp. 3411-3421.
[15] D. Arnush and F.F. Chen, "Generalized theory of helicon waves. II. Excitation and absorption," Physics of Plasmas, Vol. 5, No. 5, May 1998, pp. 1239-1254.
[16] S. Shinohara and K. Yonekura, "Discharge modes and wave structures using loop antennae in a helicon plasma source," Plasma Phys. Control. Fusion, Vol. 42, 2000, pp. 41-56.
[17] S. Shinohara and K. Shamrai, "Direct comparison of theoretical and experimental results on the antenna loading and density jumps in a high pressure helicon source," Plasma Phys. Control. Fusion, Vol. 42, 2000, pp. 865-880.